Research Square

Preprints are preliminary reports that have not undergone peer review.
They should not be considered conclusive, used to inform clinical practice,
or referenced by the media as validated information.

Plasmodium infection inhibits tumor angiogenesis through effects on tumor-associated macrophages in a murine implanted hepatoma model

Benfan Wang
University of Alberta
Qinyan Li
Guangzhou Institutes of Biomedicine and Health
Jinyan Wang
Guangzhou Institutes of Biomedicine and Health
Siting Zhao
Guangzhou Institutes of Biomedicine and Health
Bayaer Nashun
Guangzhou Institutes of Biomedicine and Health
Li Qin
Guangzhou Institutes of Biomedicine and Health
Xiaoping Chen (chen_xiaoping@gibh.ac.cn)
Guangzhou Institutes of Biomedicine and Health https://orcid.org/0000-0002-0227-6647

Research

Keywords: Plasmodium infection, Hepatocellular carcinoma, growth inhibition, tumor angiogenesis, tumor-associated macrophages, matrix metalloprotease, hemozoin

Posted Date: November 20th, 2019

DOI: https://doi.org/10.21203/rs.2.17456/v1

License: This work is licensed under a Creative Commons Attribution 4.0 International License.
Read Full License

Version of Record: A version of this preprint was published at Cell Communication and Signaling on September 24th, 2020. See the published version at https://doi.org/10.1186/s12964-020-00570-5.

Abstract

Background: Hepatocellular carcinoma (HCC) is one of the leading causes of cancer-related death in China. The lack of effective treatment results in a high recurrence rate in patients who undergo radical tumor resection, and the 5-year survival rate remains low. Our previous studies demonstrated that Plasmodium infection provides a potent antitumor effect by inducing innate and adaptive immunity in a murine Lewis lung carcinoma (LLC) model.

Methods: A study was conducted to investigate the inhibitory effect of Plasmodium infection on hepatocellular carcinoma in mice, and chip analysis techniques were used to find possible signal regulation mechanisms.

Results: we report that Plasmodium infection efficiently inhibited tumor progression and prolonged survival in tumor-bearing mice in a murine implanted hepatoma model. The inhibition of tumor progression by Plasmodium infection is related to the suppression of tumor angiogenesis within the tumor tissue and the decreased infiltration of tumor-associated macrophages (TAMs). Further study demonstrated that TAM-produced matrix metalloprotease 9 (MMP-9) contributed to tumor angiogenesis in the tumor tissue and that the reduced expression of MMP-9 in TAMs mediated by parasite infection resulted in the suppression of tumor angiogenesis. A mechanistic study revealed that the Plasmodium-derived hemozoin (HZ) that accumulated in TAMs inhibited IGF-1 signaling through the PI3-K and MAPK signaling pathways, which led to decreased expression of MMP-9 in TAMs.

Conclusions: Our study suggests that this novel method of inhibiting tumor angiogenesis by Plasmodium infection is of high importance for developing new therapies for cancer patients.

Introduction

Plasmodium infection, which causes malaria in humans or animals, has been shown to modulate host immunity by inducing the secretion of cytokines, the activation of some immune cell populations, and especially by altering the function of macrophages [1, 2]. Therefore, Greentree proposed the idea of macrophage activation-based therapeutic malaria for cancer treatment in 1981 [3]. Angsubhakorn and colleagues found that *Plasmodium* infection reduced hepatic carcinogenesis induced by dietary aflatoxin B1 [4]. Our previous study demonstrated that *Plasmodium* infection provides a potent antitumor effect through the induction of innate and adaptive antitumor immune responses in a murine Lewis lung carcinoma (LLC) model [5].

Angiogenesis plays a central role in the invasion, growth and metastasis of solid tumors through the formation of new blood vessels from preexisting vessels [6]. Blocking angiogenesis significantly inhibits tumor growth [7]. Although our previous study demonstrated that *Plasmodium* infection inhibits tumor angiogenesis by releasing plasma exosomes that contain endogenous functional microRNAs in a murine LLC model [8], the more precise mechanisms underlying the inhibition of tumor angiogenesis by *Plasmodium* infection remain unclear.

Based on a series of pilot experiments, we hypothesized that *Plasmodium* infection in tumor-bearing mice may regulate tumor angiogenesis by modulating the function of macrophages. Macrophages make up the major proportion of host-derived immune cells associated with most solid tumors and are key regulators of tumor angiogenesis [6, 9]. In the tumor microenvironment, tumor-associated macrophages (TAMs) are polarized into the alternatively activated phenotype (M2 type) and promote tumor angiogenesis through the production of several proangiogenic factors, such as matrix metalloproteinases (MMPs) [6, 9, 10]. MMP–2 and –9 are well documented to play crucial roles in the process of angiogenesis, mainly by degrading the extracellular matrix (ECM) [8, 11, 12]. A recent study showed that increased type 1 insulin-like growth factor (IGF–1) signaling is associated with an upregulation of MMP–2 and –9 expressions [13–15]. Both the Ras/Raf/ERK pathway and the PI 3-kinase/Akt signaling pathway have been shown to be crucial pathways involved in the regulation of IGF–1 functions [16–18].

Hemozoin (HZ, a malarial pigment) is a polymer of heme produced by *Plasmodium* parasites during hemoglobin degradation inside infected red blood cells (iRBCs) [19]. This pigment is released when an iRBC bursts and is rapidly engulfed by phagocytes [20]. Naturally, HZ can be engulfed by TAMs. Although in vitro studies have revealed that HZ modulates the production of inflammatory factors by murine macrophages and human monocytes [21], there is a paucity of data on the role of the modulatory effect of HZ on TAMs in the regulation of tumor development.

In the present study, we demonstrated that *Plasmodium* infection effectively inhibited tumor progression and prolonged survival in tumor-bearing mice in a murine implanted hepatoma model. The inhibition of tumor progression by *Plasmodium* infection was associated with decreased tumor angiogenesis. We further demonstrated that TAMs that produced MMP–9 contributed to tumor angiogenesis in tumor tissue and that the reduction in MMP–9 expression in TAMs mediated by infection resulted in the suppression of tumor angiogenesis. A mechanistic study revealed that the *Plasmodium*-derived HZ that accumulated in TAMs inhibited IGF–1 expression through the PI3-K and MAPK signaling pathways, which led to decreased expression of MMP–9 in the TAMs. Our study suggests a novel method of inhibiting tumor angiogenesis by *Plasmodium* infection.

Methods

Mice, cells and parasites

Female C57BL/6 mice (6–8 weeks old) were purchased from Beijing Vital River Experimental Animals, Co., Ltd. The murine Hepa1–6 hepatoma cell line was obtained from the First Affiliated Hospital of Sun Yat-Sen University and cultured in Dulbecco's modified Eagle's medium (DMEM) (GIBCO) supplemented with 10% fetal bovine serum (FBS), 1% penicillin and streptomycin. The murine H22 hepatoma cell line was purchased from the China Center for Type Culture Collection and maintained in RPMI 1640 medium supplemented with 10% FBS, 1% penicillin and streptomycin. The murine RAW264.7 macrophage cell line was kindly provided by Dr. Chiwei Huang and cultured in DMEM supplemented with 10% FBS, 1% penicillin and streptomycin. *Plasmodium yoelii 17 XNL* (*Py*)„ a strain of *Plasmodium* parasite that is

nonlethal in C57BL/6 mice, was kindly provided by BEI Resources (formerly the Malaria Research and Reference Reagent Resource Center, MR4) and was recovered in 7-week-old female C57BL/6 mice.

Design of animal experiments

To evaluate the effects of *Plasmodium* infection on tumors in mice, mice were subcutaneously inoculated with 2×10^6 Hepa1–6 or H22 cells in 100 μl of serum-free RPMI 1640 and intraperitoneally (i.p.) inoculated with 5×10^5 parasitized erythrocytes or uninfected RBCs as a control in 200 μl of saline simultaneously. The palpable spherical tumor mass emerged 4–6 days after tumor cell inoculation. The tumor size was measured every 3 or 4 days using a caliper and calculated using the formula $0.52 \times a \times b^2$ (a: long diameter of the tumor; and b: short diameter of the tumor). Blood samples were collected from the tail vein of the mice every 2 days for 30 days, and parasitemia was determined by analyzing a thin Giemsa-stained blood film. The mice were observed until death or until their tumor size reached 2000 mm^3. In some experiments, the mice were sacrificed on day 8 or 17 after parasite inoculation for biopsy. The tumor tissue was used for further analysis. For assays studying blocking parasite infection, *Plasmodium* parasites were killed with a dose of 10 mg chloroquine per kilogram of mouse body weight on day 8 after infection, and then the mice were euthanized on day 17 for further analysis.

For the orthotopic tumor model, 50 μl of 1×10^6 Hepa1–6 cells were injected into the left lobe of the liver of anesthetized mice. After recovering, the mice were i.p. inoculated with 5×10^5 parasitized erythrocytes or uninfected RBCs. On day 17 after parasite inoculation, the mice were sacrificed for biopsy. The liver and spleen were removed and photographed. The liver sections were stained with H&E.

Alginate-encapsulated tumor cell assay

An alginate-encapsulated tumor cell assay was performed in vivo as previously described with slight modifications [22]. Briefly, Hepal–6 or H22 hepatoma cells were resuspended in a 1.5% (W/V) sodium alginate solution. When the droplets were added into a swirling 37°C solution of 250 mmol/L calcium chloride, alginate beads were formed. Four alginate beads (1×10^5 Hepal–6 or H22 cells per bead) were subcutaneously implanted into an incision made on the dorsal side of mice. The mice were randomly divided into two groups (n = 10 per group). One group was i.p. inoculated with 5×10^5 parasitized erythrocytes. The other group, which acted as the control, was i.p. inoculated with the same number of uninfected RBCs. After 14 days, the mice were injected with 0.1 ml of a 100 mg/kg FITC-dextran (Sigma-Aldrich) solution via the tail vein. The beads were rapidly removed and photographed. The uptake of FITC-dextran was assessed using a standard FITC-dextran curve.

TAM isolation

Single cell suspensions were prepared from tumor tissue as described previously with some modifications [23]. Briefly, tumor-bearing mice were sacrificed 17 days after parasite inoculation. Solid tumors were chopped into small pieces and incubated with a mixture of enzymes for 30 min at 37°C. Cells were recovered by centrifugation and resuspended in PBS containing 1% FBS. The RBCs were lysed.

The tumor cells were isolated by the Ficoll density gradient method. A total of 1×10^7 cells were incubated with 10 μg of FITC- or APC-conjugated anti-F4/80 monoclonal antibody (mAb) for 30 min on ice and then washed with cold buffer to remove any unbound antibody. $F4/80^+$ cell populations were sorted by flow cytometry (BD FACSAria). The purity of the cell populations was between 85 and 90%.

TAM induction in vitro

TSN was obtained by culturing 4×10^6 Hepa1–6 cells in 24-well flat-bottom tissue culture plates for 72 h. For the in vitro induction of the TAM phenotype, 5×10^5 RAW 264.7 cells were seeded in a six-well plate, and the TSN (1:2 dilution) was added. After 48 h, total RNA was isolated, and the expression levels of alternatively activated genes (*ym1, mgl1/2,* and *arginase 1)* and classical activated genes (*il–12, inos)* were analyzed.

Microarray experiment

Hepa1–6 cell-implanted mice were sacrificed on day 17 after *Plasmodium* infection. TAM isolation was performed as described in a previous section.The TAMs were sorted by FACS using FITC-conjugated anti-F4/80 mAb. Gene expression was compared using Roche NimbleGen mouse gene chips (CapitalBio, China). Genes that showed an expression fold-change ≥ 2 with a q-value ≤ 0.05 in triplicate arrays were considered to be significantly induced in response to treatment. These differentially expressed genes were annotated using the Molecule Annotation System (CapitalBio, China).

Immunohistochemistry

Paraffin-embedded tissue sections were deparaffinized in xylene and rehydrated through a graded series of ethanol. High-pressure antigen retrieval was performed in 10 mM EDTA buffer (pH 8.0) before the sections were incubated with a primary antibody against F4/80, a rat mAb against mouse macrophages (clone No. RM0029–11H3), an anti-CD31 antibody and an anti-MMP–9 antibody. Bright field images were captured and analyzed.

The number of TAMs, density of CD31-positive microvessels and expression of MMP–9 in TAMs were assessed under 400× magnification (0.17 mm^2 field) in 8 random fields, and the results are expressed as the mean number per field ± SD (8 fields per tumor, four tumors per group).

RNA isolation and real-time RT-PCR

Total RNA was isolated using Trizol (Invitrogen) according to the manufacturer's instructions. Real-time RT-PCR for the *ym1, arg–1, mgl1, mgl2, fizz1, inos, mmp–2, mmp–9, leyve1, vegf, igf1* and *-actin* genes was performed on an MJ chromo 4 real-time PCR machine (Bio-Rad) using the OneStep SYBR® PrimeScript™ RT-PCR Kit (Takara) according to the manufacturer's instructions. The *-actin* gene was used as a reference gene.

Western blot analysis

Sample preparations from tissue or cells, gel electrophoresis, and transfer to polyvinylidene fluoride membranes (Millipore) were carried out as described previously [23]. The membranes were incubated with primary antibodies against MMP–2/9, VEGF, IGF–1, AKT, phospho-AKT, p44/42 MAPK (Erk1/2), and phospho-p44/42 MAPK (Erk1/2) at 4°C overnight and with secondary antibodies at room temperature for 1 h. Immobilon Western HRP Chemiluminescent Substrate (Cell Signaling Technology) was used to detect the specific signals. Band intensity was visualized.

Preparation of HZ

Natural HZ was obtained from the spleen and liver of *Py*-infected C57BL/6 mice. Tissues were lysed using saponin. HZ was recovered via centrifugation, washing, and processing with a proteinase, nuclease and urea mixture. The pigment was lyophilized, dried, resuspended in endotoxin-free PBS at a final concentration of 10 mg/ml and kept at −20℃. The endotoxin level of the isolated HZ was assessed using a *Limulus amebocyte* lysate kit (Sigma-Aldrich). The endotoxin level was less than 0.015 EU.

Assessment of IGF–1 derived from HZ-loaded TAMs

To assess the effect of HZ on the secretion of IGF–1, induced TAMs were treated with HZ (100 μg/ml) or left untreated for 48 h. The IGF–1 mRNA and protein levels were evaluated using real-time PCR and immunoblot analysis, respectively. In some experiments, the cells were treated with different concentrations of HZ (10 to 200 μg/ml) and for different times (3 to 48 h).

Preparation of Cl_2MDP liposomes and the macrophage "in vivo knockout" assay

These experiments were performed by following a previously described procedure [10].

Statistical analysis

The statistical significance of the differences between values was determined by Student's t test using GraphPad Prism 6.01 software. The correlation between two factors was evaluated by Pearson's correlation analysis. Kaplan-Meier survival curves were plotted. Data are expressed as the mean ± SD. *P* values < 0.05 were considered significant.

Results

Plasmodium Infection Inhibited the Growth of Liver Cancer Cells and Prolonged the Survival of Tumor-Bearing Mice

To observe the effect of *Plasmodium* infection on tumor growth, mice simultaneously received a subcutaneous (s.c.) injection of Hepa1–6 or H22 cells and an intraperitoneal injection of the malarial parasite. The tumor growth and survival rates of tumor-bearing mice were evaluated. As shown in Fig. 1A, *Plasmodium* infection significantly inhibited tumor growth in the Hepa1–6 cell-implanted hepatoma model. The survival rate of the tumor-bearing mice in the infected group was significantly higher than

that of the tumor-bearing mice in the uninfected control group (Fig. 1B). Considering the potential side effect of *Plasmodium* infection, parasitemia was monitored by thin Giemsa-stained blood film microscopy. The parasite densityappeared to peak on days 16 to 24 and then decreased to a low level until it disappeared after 32 days (Fig. S1).

The inhibitory effect of *Plasmodium* infection on tumor growth was also observed in the H22 cell-implanted hepatoma model (Fig. 1C). The survival rate of the tumor-bearing mice in the infected group was also significantly higher than that of the tumor-bearing mice in the control group (Fig. 1D).

To further validate the inhibitory effect of *Plasmodium* infection on tumor growth, we performed a similar experiment using an orthotopically implanted tumor model. A similar result was obtained through gross observation of the removed tumors (Fig. 1E) and microscopic observation of hematoxylin and eosin (H&E)-stained tumor tissue (Fig. 1F, left panel). Compared with the control group, the infected group exhibited significantly reduced tumor nodule formation in the liver (Fig. 1F, right panel).

Plasmodium Infection Suppressed Tumor Angiogenesis

It is worth noting that in the *Plasmodium*-infected tumor-bearing mice, tumor angiogenesis was significantly inhibited while tumor growth was inhibited (Fig. 2A). Consistent with this result, H&E staining and CD31 immunohistochemical staining of the tumors from tumor-bearing mice on day 17 after the parasite infection showed that tumor angiogenesis was significantly decreased in the infected mice compared to the control mice (Fig. 2B and 2C).

To further confirm whether *Plasmodium* infection may lead to the inhibition of angiogenesis in tumor-bearing mice, an alginate-encapsulated tumor cell assay was carried out. As shown in Fig. 2D, angiogenesis in the hepatoma tissue of the Hepa1–6 cell-implanted mice infected with the parasite was markedly inhibited. FITC-dextran uptake in the tumor-bearing mice infected with the parasite was significantly lower than that in the control mice (Fig. 2E). Together, these results showed that *Plasmodium* infection induced an important reduction in tumor angiogenesis in the tumor-bearing mice, leading to the inhibition of tumor growth.

Suppression of TAMs Mediated by Plasmodium Infection Contributes to the Inhibition of Tumor Angiogenesis

TAMs have been reported to be important promoters of tumor angiogenesis in the tumor microenvironment [6]. To determine the effect of TAMs on tumor angiogenesis in the *Plasmodium* infection model, we analyzed the infiltration of TAMs into the tumor tissue on days 8 and 17 after the infection. Immunohistochemical staining showed that compared with the control treatment, *Plasmodium* infection significantly decreased the number of TAMs on days 8 and 17 after infection (Fig. 3A and 3B; Fig. S2). Furthermore, the proportion of TAMs was approximately 11% in the uninfected tumor-bearing controls, whereas the proportion was markedly decreased to approximately 5% in the tumor-bearing mice

on day 17 after the parasite infection (Fig. 3C). Examination of the absolute number of TAMs revealed that the parasite infection significantly reduced the number of infiltrating TAMs (Fig. 3D).

Our previous study demonstrated that the reduction in TAM infiltration induced by treatment with dichloromethylene diphosphonate (Cl_2MDP) liposomes led to an improvement in the tumor microenvironment and a significant inhibition of tumor growth [10]. To further confirm that a reduction in TAM infiltration may induce the inhibition of tumor angiogenesis, we designed a TAM "in vivo-knockdown" assay by treating tumor-bearing mice with Cl_2MDP liposomes. Compared to the phosphate-buffered saline (PBS) liposome-treated tumors, the tumors treated with Cl_2MDP liposomes showed obviously reduced blood vessel density and CD31 expression (Fig. 3E). Consistent with this result, the number of MF+ macrophages in the tumors treated with Cl_2MDP liposomes was also significantly decreased (Fig. 3F). Moreover, an analysis of the correlation between the expression of CD31 and that of MF molecules in the tumor microenvironment of the Cl_2MDP liposome-treated tumor-bearing mice revealed that the extent of tumor angiogenesis was positively correlated with the number of infiltrating TAMs in the tumor (Fig. 3G). Interestingly, compared to the uninfected control group, the infected group exhibited reductions in both tumor angiogenesis and TAM infiltration (Fig. 3H and 3I).

Taken together, our data indicated that TAMs contribute to tumor angiogenesis, which is inhibited by *Plasmodium* infection.

Plasmodium Infection Reduced the Expression of IGF–1 and MMP–9 in TAMs

To explore the underlying mechanism by which *Plasmodium* infection inhibits tumor angiogenesis mediated by TAMs, we sorted the TAMs from the murine tumors and performed gene chip analysis. The purity of the sorted TAMs was shown to be approximately 90% (Fig. S3A). As expected, compared to the control group, the infected group exhibited markedly changed TAM gene expression (Fig. 4A, Fig. S3B). Importantly, the gene expression profiles related to angiogenesis were significantly different between the two groups. In the infected group, the expression of proangiogenic genes such as *mmp–2/9* and *igf–1* was lower, while the expression of antiangiogenic genes such as *Nppb* was higher than that in the control group. Unexpectedly, the *vegf* gene in TAMs showed a slight reduction in the infected group (Fig. 4B). Pathway analysis showed that *igf–1* was a key upstream regulator of *mmp–2/9.* These results were further confirmed by RT-PCR analyses and Western blot validation. As expected, the RNA and protein levels of *mmp–9* in the TAMs from parasite-infected tumors were significantly lower than those in the TAMs from control group tumors. The levels of *igf–1* RNA and IGF–1 protein were also reduced approximately 4-fold in the infected mice (Fig. 4C and 4D), although the level of mmp–2 showed only a slight reduction (Fig. S3C). These results suggested that the reduction in MMP–9 and IGF–1 expression in TAMs induced by *Plasmodium* infection might be responsible for the reduced tumor angiogenesis.

To further investigate the concentrations of MMP–9 and IGF–1 within the tumor microenvironment, we also analyzed the tumor tissue 17 days after *Plasmodium* infection. Consistent with the expression in TAMs, MMP–9 and IGF–1 expression was also significantly decreased in the infected tumor tissue (Fig.

4E and 4F); however, the expression of VEGF was only slightly decreased in the infected tumors compared with the uninfected tumors (Fig. S3C). In addition, the results from a FACS-like tissue cytometry analysis confirmed that MMP–9 expression in the *Plasmodium*-infected group was significantly lower than that in the control group (Fig. 4G, Fig. S4). Taken together, these results suggested that *Plasmodium* infection may reduce MMP–9 and IGF–1 expression in TAMs and tumor tissue and that this effect is responsible for the reduced angiogenesis within the tumors.

The Number of TAMs and MMP–9 Expression Positively Correlated with Tumor Vascular Density

Immunohistochemical analysis revealed that the cells secreting MMP–9 were mainly localized in the tumor margin, and most of these cells were macrophages (Fig. 4H). Next, we carried out correlation analyses by using the expression of MMP–9, CD31 and MF molecules in the *Plasmodium*-infected model measured by immunohistochemical analysis. Pearson's correlation test showed that MMP–9, the number of infiltrating TAMs, and the degree of angiogenesis achieved quantitatively similar positive correlations in the parasite-infected group (Fig. S5A) and the uninfected group (Fig. S5B). Furthermore, similar results were achieved quantitatively when the two groups were combined together (Fig. 4I). Taken together, these results suggested that the reduction in MMP–9 expression in the TAMs significantly correlated with the inhibition of tumor angiogenesis in the *Plasmodium*-infected model.

Plasmodium Infection Reduced IGF–1 Expression by Blocking IGF–1R Signaling and the PI3-K and MAPK Pathways

IGF–1 has been reported to promote MMP–9 expression via the AKT and MEK/ERK pathways [13–16]. We next conducted a mechanistic study to explore the role of IGF signaling in the expression of MMP–9 in *Plasmodium*-infected tumor-bearing mice. There was a significant reduction in the p-AKT and phosphorylated p42/44 MAPK levels in the infected group compared with the uninfected group (Fig. 5A and 5B). Terminating the parasite infection restored the expression of these signaling proteins (Fig. 5C and 5D), implying that both the PI3-K and MAPK pathways participate in the IGF–1 signaling that induces MMP–9 expression.

HZ, a Plasmodium Metabolite, Reduced the Expression of IGF–1 in TAMs

As expected, *Plasmodium*-infected red blood cells (iRBCs) were found within the tumors from the tumor-bearing mice (Fig. 6A, upper panel). Interestingly, we observed that HZ, a metabolite of the *Plasmodium* parasite, accumulated in TAMs (Fig. 6A, down panel). Thus, we postulated that HZ could play roles in the modulation of the expression of IGF–1 in TAMs.

To confirm this hypothesis, we examined the expression of IGF–1 molecules in polarized M2-like macrophages stimulated with HZ. To generate M2-like macrophages, RAW264.7 cells were cocultured with Tumor cell-free supernatant (TSN) in vitro. These polarized cells showed enhanced expression of genes such as *ym1, fizzl, mgl1, arginase–1 (arg–1)* and *vegf,* but the expression of *inos,* a gene that correlates with classical activation, was downregulated (Fig. 6B). Furthermore, these polarized M2-like

macrophages could phagocytose HZ in vitro (Fig. 6C), and cell viability was not affected by the doses of HZ used.

Polarized M2-like macrophages were treated with HZ for 48 h, and the expression of the *igf–1* gene was examined. As shown in Fig. 6D and 6E, the expression of IGF–1 significantly decreased when the M2-like macrophages phagocytosed HZ. Interestingly, the expression of IGF–1 was reduced in a dose-dependent fashion (Fig. 6F). Compared with the dose at 10 μg/ml, the dose of HZ at 100 μg/ml showed a much stronger suppression of this gene expression in the M2-like cells. However, when the M2-like cells were treated with HZ (100 μg/ml) for the indicated time periods shown in Fig. 6G, the change in IGF–1 expression was dependent on the treatment time. Together, these results showed that HZ played an important role in the reduced expression of IGF–1 in the TAMs of the *Plasmodium*-infected tumor-bearing mice.

Discussion

In the present study, we showed that *Plasmodium* infection efficiently inhibits hepatic tumor progression via the inhibition of tumor angiogenesis mediated by TAMs. Mechanistic studies revealed that the *Plasmodium* product HZ, which is taken up by TAMs, down-regulates MMP–9 expression by suppressing IGF–1 via the PI3-K and MAPK pathways.

For a long time, it has been recognized that parasite infection may serve to enhance immune surveillance mechanisms against some types of solid cancers [5, 8, 24]. Furthermore, our global epidemiological data analysis also suggested an inverse correlation between malaria incidence and cancer mortality [24]. *Plasmodium* pathogen-associated molecular patterns (PAMPs), such as glycosylphosphatidylinositol (GPI) anchors, HZ and immunostimulatory nucleic acid motifs [25], can be recognized by host immune cell sensors called pattern recognition receptors (PRRs) [26, 27], triggering systemic immune responses that counteract the immunosuppressive tumor microenvironment that contains TGF-β, IL–10, regulatory T cells and myeloid-derived suppressive cells (MDSCs), thereby contributing to the suppression of tumor development [28, 29]. Indeed, our previous study demonstrated that blood-stage malaria exerts antitumor effects by inducing a potent antitumor innate immune response that includes the secretion of IFN-γ and the activation of natural killer (NK) cells. Our murine lung cancer model studies also demonstrated that malaria infection induced adaptive antitumor immunity by increasing the proliferation of tumor-specific T cells, the cytolytic activity of CD8+ T cells and the infiltration of these cells into tumor tissue [5]. A study by Deng and colleagues demonstrated that the inoculation of attenuated liver-stage *Plasmodium* induces an antitumor innate immune response, including the secretion of tumor necrosis factor (TNF)-α, IL–6/12 and IFN-γ and antitumor adaptive immunity with increasing CD8+ T cell cytolytic activity [30].

Macrophages or TAMs derived from circulating monocytes are often the most abundant immune cells in the tumor microenvironment and are key regulators of tumor progression [9, 10, 31]. Our previous study showed that TAM depletion mediated by clodronate liposomes inhibits hepatic tumor growth [9]. Indeed, the role of TAMs in promoting hepatoma growth has been confirmed by several clinical investigations

[32, 33]. Therefore, in the present study, we focused on investigating the role of TAMs in tumor angiogenesis in tumor-bearing mice infected with *Plasmodium.*

Accumulating evidence indicates that TAMs release a panel of potent proangiogenic cytokines and growth factors, such as VEGF, TNFα, IL–8, basic fibroblast growth factor, thymidine phosphorylase, urokinase-type plasminogen activator, adrenomedullin, semaphoring 4D, and cyclooxygenase–2[34–36]. VEGF is known to be a major proangiogenic cytokine released by TAMs that causes an angiogenic switch. Its levels correlate with TAM density and tumor angiogenesis in several types of human cancer [37]. However, our present study showed no significant decrease in the VEGF levels of the TAMs in the *Plasmodium*-infected tumor-bearing mice, which suggests that there might be other antiangiogenic mechanisms. Several studies have demonstrated that TAMs may produce some angiogenesis-related enzymes, including MMP–2 and MMP–9, which mediate ECM degradation and increase the vascular invasion of tumor cells [38, 39]. The inhibition of MMP–9 expression by infiltrating macrophages via zoledronic acid effectively diminishes angiogenic responses in cervical cancer cells [40]. Similar to this finding, our study confirmed that TAMs that infiltrated into the tumor tissue of tumor-bearing mice are an important source of MMP–9 in the tumor environment. The decrease in MMP expression in TAMs can be an important mechanism for the inhibition of tumor angiogenesis in *Plasmodium*-infected tumor-bearing mice. The IGF/IGF-IR axis is considered to play an important role in the regulation of several MMPs and can thereby trigger MMP-mediated tumor angiogenesis and invasion [14, 15, 41, 42]. IGF–1 has been shown to signal intracellularly through the PI3 and MAPK pathways after binding to IGF–1R on the cell surface, and IGF–1 thereby increases the enzymatic activity of MMP–2 and MMP–9 and enhances the proliferation and migration of tumor cells [14, 15, 43–45]. Noticeably, IGF–1 derived from polarized macrophages can maintain the M2-type activation profile in these macrophages by activating the PI3-K and MAPK pathways [43, 46]. We showed that infection with *Plasmodium* significantly inhibited tumor angiogenesis by inhibiting the expression of MMP–9 in TAMs. The reduced expression of MMP–9 in TAMs was mediated by suppressing IGF–1 via the PI3-K and MAPK pathways. These data suggested that *Plasmodium* could alter the angiogenic functions of TAMs by regulating particular signal transduction pathways.

Plasmodium-infected RBCs (iRBCs) were observed within the tumor vasculature in the animals. Thus, the iRBCs and *Plasmodium* metabolic products including HZ could be easily phagocytosed by TAMs. It has been suggested that the consequence of TAM phagocytosis may be the direct alteration of the activation status of the TAM, resulting in decreased infiltration of the TAM into tumor sites. Alternatively, the engulfment of *Plasmodium* metabolic products induces apoptosis in TAMs that may lead to a partial depletion of TAMs. We have demonstrated that the decreased number of TAMs at least partially contributes to the inhibition of tumor angiogenesis. Additionally, our study showed that the phagocytosis of HZ by TAMs induces a significant reduction in the production of IGF–1, although the mechanism has to be elucidated.

Overall, the present study demonstrated that *Plasmodium* infection inhibits hepatic tumor progression by reducing TAM-mediated tumor angiogenesis (Fig. 7). *Plasmodium* infection suppresses the infiltration of

TAMs into tumors, which can alter the tumor milieu and thereby partially contribute to the inhibition of tumor angiogenesis. More importantly, infection can significantly reduce the levels of proangiogenic factors and increase the levels of antiangiogenic factors in TAMs. In particular, infection can significantly decrease MMP–9 expression by regulating IGF–1, which may signal intracellularly through the PI3 and MAPK pathways after binding to IGF–1R on the cell surface and thereby increase the expression of MMPs in tumor-bearing mice.

Considering the findings of our previous studies [5, 8, 24, 47], which showed that *Plasmodium* parasite infection induces antitumor immunity and inhibits tumor angiogenesis in animal models of cancer, we conclude that *Plasmodium* infection or component vaccination provides a potent therapeutic strategy for cancer treatment. Three clinical trials of *Plasmodium* immunotherapy for advanced lung cancer (clinicaltrials.gov/ct2/show/NCT02786589), advanced breast and liver cancers (clinicaltrials.gov/ct2/show/NCT03474822), and advanced cancers (clinicaltrials.gov/ct2/show/NCT03375983) have been approved and are ongoing in China. In these clinical trials, our collaborators have observed that infection with blood-stage *Plasmodium vivax* (a relatively benign form of the human malaria parasite) activates the immune system of advanced cancer patients without severe side effects or complications because artemisinin effectively controls parasitemia at a safe level (unpublished data). A gene-modified attenuated human malaria parasite could be explored as a cancer vaccine vector or an immunotherapy for cancer patients [47].

Conclusions

In conclusion, we highlighted in this study that the immunity mediated by *Plasmodium* infection can reactivate the immunity inhibited by tumors. Macrophages infiltrating in tumor microenvironment bridge the gap between these two different immune mechanisms. This novel method of inhibiting tumor angiogenesis by *Plasmodium* infection is of high importance for developing new cancer therapy strategies in future.

Abbreviations

TAMs: Tumor-associated Macrophages

MDSCs: Myeloid-derived Suppressive Cells *NK:* natural killer

HCC: Hepatocellular carcinoma *LLC:* Lewis Lung Carcinoma

HZ: hemozoin

iRBCs: Infected Red Blood Cells

i.p.: intraperitoneally *s.c.:* subcutaneous

W/V: Weight versus Volume

FITC: Fluorescein Isothiocyanate

FBS: Fetal Bovine Serum *EDTA:* Ethylenediaminetetraacetic Acid

MAb: Monoclonal Antibody

IGF–1: Type 1 Insulin-like Growth Factor

Nppb: Natriuretic Peptide B *TNF:* tumor necrosis factor *IFN:* Interferon

MMP: Matrix Metalloprotease *ym1:* chitinase-like 3 *arg–1:* Arginase 1

mgl: macrophage galactose-type C-type lectin

fizz1: Esistin Like Alpha IL: Interleukins

inos: Inducible Nitric Oxide Synthase *vegf:* Vascular Endothelial Growth Factor

leyve1: Lymphatic Vessel Endothelial Hyaluronan Receptor 1

Cl2MDP: Dichloromethylene Diphosphonate *PBS:* Phosphate-buffered Saline

MAPK: Mitogen-activated Protein Kinase *PI3-K:* Phosphoinositide 3-kinase

AKT: AKT serine/threonine kinase 1 *p- AKT:* Phospho-Akt serine/threonine kinase

PAMPs: pathogen-associated molecular patterns *GPI:* Glycosylphosphatidylinositol

Declarations

Ethics approval and consent to participate

All animal experiments were carried out in accordance with the Guidance for the Care and Use of Laboratory Animals guidelines created by the Institutional Animal Care and Use Committee of Guangzhou Institutes of Biomedicine and Health (IACUC-GIBH), and all animal experiment protocols were approved by the committee.

Consent for publication

Full consent for the publication of mouse experimental data was obtained.

Availability of data and materials

The datasets generated and analyzed during this study are available from the corresponding author on reasonable request.

Competing interests

The authors declare that they have no financial or commercial conflicts of interest.

Funding

This work was supported by National Key R & D Program of China (Grant No. 2016YFE0107300 and National Natural Science Foundation of China (NSFC, No. 81673003).

Authors' contributions

BW, LQ, JW, and XC designed the project, analyzed the data and wrote the manuscript. BW participated in all parts of the experiments. QL, BN, and SZ participated in the animal experiments. All authors read and approved the final manuscript.

Acknowledgments

We would like to thank Weifang Hu, Nangzheng Peng, Songlin Yu, Renli Ru, Zhu Tao, Cuizhu Huang and Yayong Li for their technical support. We thank Dr. Chiwai Huang for kindly providing the RAW264.7 macrophage cell line. We thank MR4 for the provision of parasite material.

References

1.Artavanis-Tsakonas K, Tongren JE, Riley EM. The war between the malaria parasite and the immune system: immunity, immunoregulation and immunopathology. Clin Exp Immunol. 2003;133:145–52.

2.Stevenson MM, Riley EM. Innate immunity to malaria. Nat Rev Immunol. 2004;4:169–80.

3.Greentree LB. Malariotherapy and cancer. Med Hypotheses. 1981;7:43–9.

4.Angsubhakorn S, Bhamarapravati N, Sahaphong S, Sathiropas P. Reducing effects of rodent malaria on hepatic carcinogenesis induced by dietary aflatoxin B1. Int J Cancer. 1988;41:69–73.

5.Chen L, He Z, Qin L, Li Q, Shi X, Zhao S, et al. Antitumor effect of malaria parasite infection in a murine Lewis lung cancer model through induction of innate and adaptive immunity. PLoS One. 2011;6:e24407.

6.Dirkx AE, Oude Egbrink MG, Wagstaff J, Griffioen AW. Monocyte/macrophage infiltration in tumors: modulators of angiogenesis. J Leukoc Biol. 2006;80:1183–96.

7.Klein G, Vellenga E, Fraaije MW, Kamps WA, de Bont ES. The possible role of matrix metalloproteinase (MMP)–2 and MMP–9 in cancer, e.g. acute leukemia. Crit Rev Oncol Hematol. 2004;50:87–100.

8.Yang Y, Liu Q, Lu J, Adah D, Yu S, Zhao S, et al. Exosomes from Plasmodium-infected hosts inhibit tumor angiogenesis in a murine Lewis lung cancer model. Oncogenesis. 2017;6:e351.

9.Lin EY, Li JF, Gnatovskiy L, Deng Y, Zhu L, Grzesik DA, et al. Macrophages regulate the angiogenic switch in a mouse model of breast cancer. Cancer Res. 2006;66:11238–46.

10.Wang B, Li Q, Qin L, Zhao S, Wang J, Chen X. Transition of tumor-associated macrophages from MHC class II(hi) to MHC class II(low) mediates tumor progression in mice. BMC Immunol. 2011;12:43.

11.Masson V, de la Ballina LR, Munaut C, Wielockx B, Jost M, Maillard C, et al. Contribution of host MMP–2 and MMP–9 to promote tumor vascularization and invasion of malignant keratinocytes. FASEB J. 2005;19:234–6.

12.John A, Tuszynski G. The role of matrix metalloproteinases in tumor angiogenesis and tumor metastasis. Pathol Oncol Res. 2001;7:14–23.

13.Zhang D, Samani AA, Brodt P. The role of the IGF-I receptor in the regulation of matrix metalloproteinases, tumor invasion and metastasis. Horm Metab Res. 2003;35:802–8.

14.Mira E, Manes S, Lacalle RA, Marquez G, Martinez AC. Insulin-like growth factor I-triggered cell migration and invasion are mediated by matrix metalloproteinase–9. Endocrinology. 1999;140:1657–64.

15.Saikali Z, Setya H, Singh G, Persad S. Role of IGF–1/IGF–1R in regulation of invasion in DU145 prostate cancer cells. Cancer Cell Int. 2008;8:10.

16.Chattopadhyay S, Shubayev VI. MMP–9 controls Schwann cell proliferation and phenotypic remodeling via IGF–1 and ErbB receptor-mediated activation of MEK/ERK pathway. Glia. 2009;57:1316–25.

17.Samani AA, Brodt P. The receptor for the type I insulin-like growth factor and its ligands regulate multiple cellular functions that impact on metastasis. Surg Oncol Clin N Am. 2001;10:289–312, viii.

18.Hanahan D, Weinberg RA. The hallmarks of cancer. Cell. 2000;100:57–70.

19.Egan TJ. Haemozoin formation. Mol Biochem Parasitol. 2008;157:127–36.

20.Diou J, Gauthier S, Tardif MR, Fromentin R, Lodge R, Sullivan DJ, Jr., et al. Ingestion of the malaria pigment hemozoin renders human macrophages less permissive to HIV–1 infection. Virology. 2009;395:56–66.

21.Jaramillo M, Plante I, Ouellet N, Vandal K, Tessier PA, Olivier M. Hemozoin-inducible proinflammatory events in vivo: potential role in malaria infection. J Immunol. 2004;172:3101–10.

22.Hoffmann J, Schirner M, Menrad A, Schneider MR. A highly sensitive model for quantification of in vivo tumor angiogenesis induced by alginate-encapsulated tumor cells. Cancer Res. 1997;57:3847–51.

23.Kusmartsev S, Gabrilovich DI. STAT1 signaling regulates tumor-associated macrophage-mediated T cell deletion. J Immunol. 2005;174:4880–91.

24.Qin L, Chen C, Chen L, Xue R, Ou-Yang M, Zhou C, et al. Worldwide malaria incidence and cancer mortality are inversely associated. Infect Agent Cancer. 2017;12:14.

25.Liehl P, Zuzarte-Luis V, Chan J, Zillinger T, Baptista F, Carapau D, et al. Host-cell sensors for Plasmodium activate innate immunity against liver-stage infection. Nat Med. 2014;20:47–53.

26.O'Neill LA, Golenbock D, Bowie AG. The history of Toll-like receptors - redefining innate immunity. Nat Rev Immunol. 2013;13:453–60.

27.Barbalat R, Ewald SE, Mouchess ML, Barton GM. Nucleic acid recognition by the innate immune system. Annu Rev Immunol. 2011;29:185–214.

28.Gazzinelli RT, Kalantari P, Fitzgerald KA, Golenbock DT. Innate sensing of malaria parasites. Nat Rev Immunol. 2014;14:744–57.

29.van der Burg SH, Arens R, Ossendorp F, van Hall T, Melief CJ. Vaccines for established cancer: overcoming the challenges posed by immune evasion. Nat Rev Cancer. 2016;16:219–33.

30.Deng X, Zheng H, Zhou D, Liu Q, Ding Y, Xu W, et al. Antitumor effect of intravenous immunization with malaria genetically attenuated sporozoites through induction of innate and adaptive immunity. Int J Clin Exp Pathol. 2016;9:978–86.

31.Pollard JW. Tumour-educated macrophages promote tumour progression and metastasis. Nat Rev Cancer. 2004;4:71–8.

32.Kuang DM, Zhao Q, Peng C, Xu J, Zhang JP, Wu C, et al. Activated monocytes in peritumoral stroma of hepatocellular carcinoma foster immune privilege and disease progression through PD-L1. J Exp Med. 2009;206:1327–37.

33.Kuang DM, Peng C, Zhao Q, Wu Y, Zhu LY, Wang J, et al. Tumor-activated monocytes promote expansion of IL–17-producing CD8+ T cells in hepatocellular carcinoma patients. J Immunol. 2010;185:1544–9.

34.Sica A, Mantovani A. Macrophage plasticity and polarization: in vivo veritas. J Clin Invest. 2012;122:787–95.

35.Chen P, Huang Y, Bong R, Ding Y, Song N, Wang X, et al. Tumor-associated macrophages promote angiogenesis and melanoma growth via adrenomedullin in a paracrine and autocrine manner. Clin

Cancer Res. 2011;17:7230–9.

36.Sierra JR, Corso S, Caione L, Cepero V, Conrotto P, Cignetti A, et al. Tumor angiogenesis and progression are enhanced by Sema4D produced by tumor-associated macrophages. J Exp Med. 2008;205:1673–85.

37.Shieh YS, Hung YJ, Hsieh CB, Chen JS, Chou KC, Liu SY. Tumor-associated macrophage correlated with angiogenesis and progression of mucoepidermoid carcinoma of salivary glands. Ann Surg Oncol. 2009;16:751–60.

38.Lewis CE, Pollard JW. Distinct role of macrophages in different tumor microenvironments. Cancer Res. 2006;66:605–12.

39.Mason SD, Joyce JA. Proteolytic networks in cancer. Trends Cell Biol. 2011;21(4):228–37.

40.Giraudo E, Inoue M, Hanahan D. An amino-bisphosphonate targets MMP–9-expressing macrophages and angiogenesis to impair cervical carcinogenesis. J Clin Invest. 2004;114:623–33.

41.Stawowy P, Kallisch H, Kilimnik A, Margeta C, Seidah NG, Chretien M, et al. Proprotein convertases regulate insulin-like growth factor 1-induced membrane-type 1 matrix metalloproteinase in VSMCs via endoproteolytic activation of the insulin-like growth factor–1 receptor. Biochem Biophys Res Commun. 2004;321:531–8.

42.Yoon A, Hurta RA. Insulin like growth factor–1 selectively regulates the expression of matrix metalloproteinase–2 in malignant H-ras transformed cells. Mol Cell Biochem. 2001;223:1–6.

43.Zhang M, Liu J, Li M, Zhang S, Lu Y, Liang Y, et al. Insulin-like growth factor 1/insulin-like growth factor 1 receptor signaling protects against cell apoptosis through the PI3K/AKT pathway in glioblastoma cells. Exp Ther Med. 2018;16:1477–82.

44.Liu L, Wang X, Li X, Wu X, Tang M. Upregulation of IGF1 by tumor-associated macrophages promotes the proliferation and migration of epithelial ovarian cancer cells. Oncol Rep. 2018;39:818–26.

45.Samani AA, Yakar S, LeRoith D, Brodt P. The role of the IGF system in cancer growth and metastasis: overview and recent insights. Endocr Rev. 2007;28:20–47.

46.Roszer T. Understanding the Mysterious M2 Macrophage through Activation Markers and Effector Mechanisms. Mediators Inflamm. 2015;2015:816460.

47.Liu Q, Yang Y, Tan X, Tao Z, Adah D, Yu S, et al. Plasmodium parasite as an effective hepatocellular carcinoma antigen glypican–3 delivery vector. Oncotarget. 2017;8:24785–96.

Figures

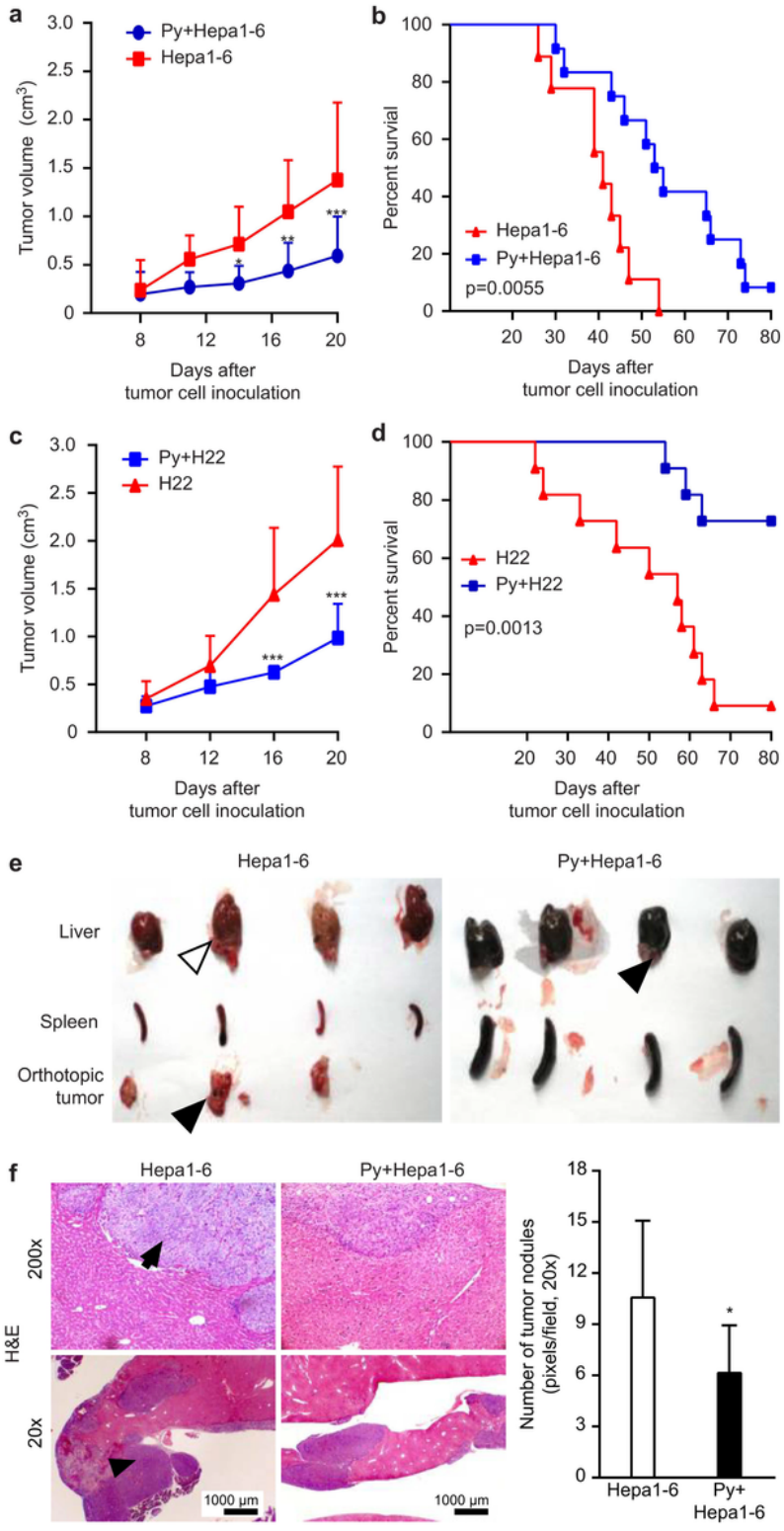

Figure 1

Plasmodium infection inhibited tumor progression and prolonged survival in tumor-bearing mice. (A-D) Hepa1-6 (A, B) or H22 (C, D) cells were s.c. inoculated into C57BL/6 mice, and Plasmodium parasites were simultaneously inoculated i.p. (n=12). The tumor sizes and survival of the mice were monitored. The data are representative of three independent experiments. The columns represent the mean ± SD. Statistical analysis was performed using GraphPad Prism software 6.0 (two-way analysis of variance

(ANOVA)). **, p <0.01; ***, p <0.001. (E-F) Hepa1-6 cells were injected into the liver of mice, and parasites were i.p. inoculated (n=10). Seventeen days later, the liver, spleen and orthotopic tumor (black arrow) were removed and photographed (E). The nodules (black arrow) in the liver were observed by H&E staining and imaged (F, left panel). Original magnification: 400×. Quantitative analysis was performed by counting the number of nodules with the same original magnification (200×) (F, right panel).

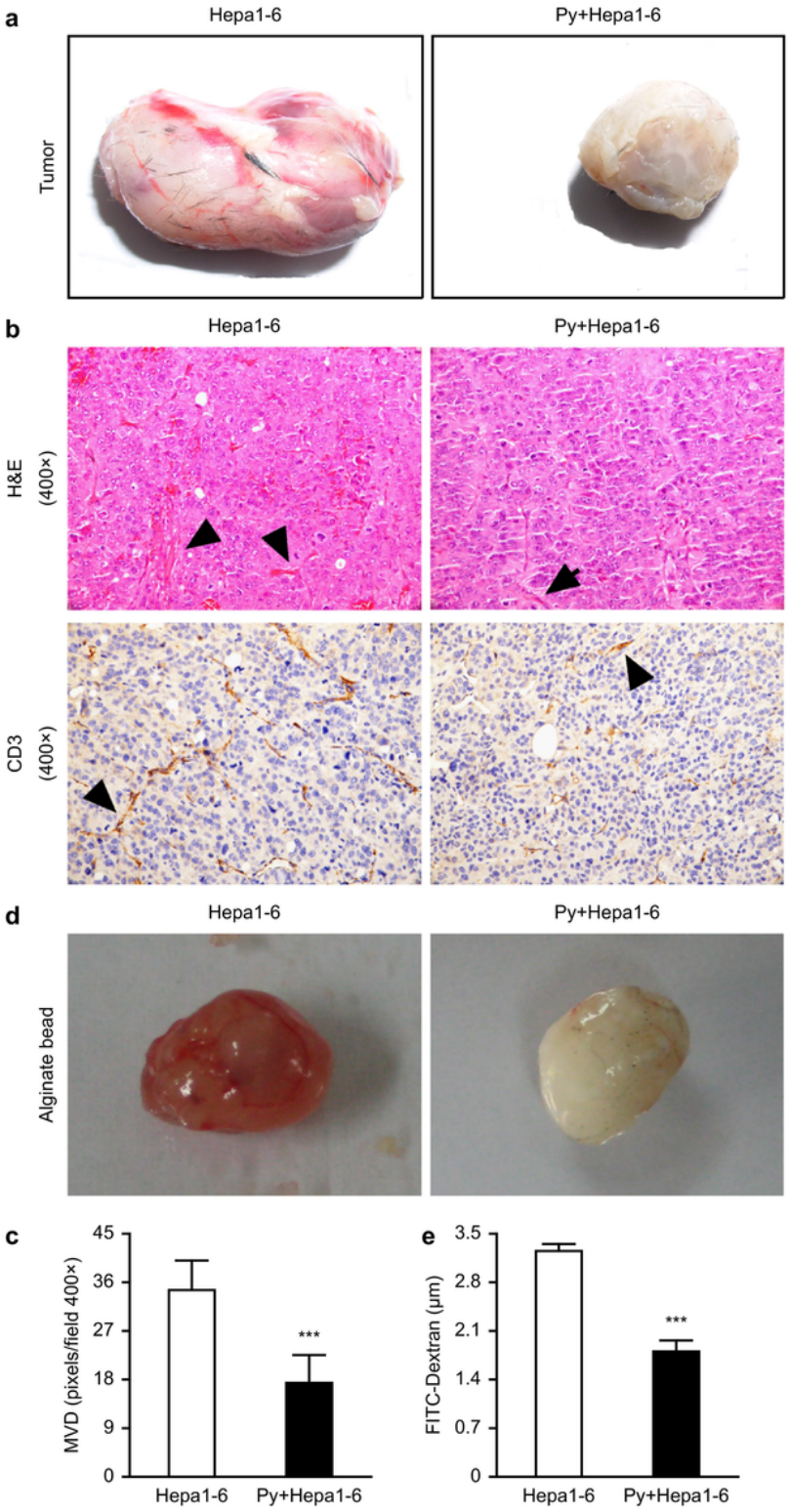

Figure 2

Plasmodium infection suppressed neovascularization in Hepa1-6-implanted tumor tissue (A-C) The vascularization of the tumor tissue from tumor-bearing mice on day 17 after Plasmodium infection was imaged (n=4) (A). H&E staining showed the neovascularization of the tumor in tumor-bearing mice on day 17 after Plasmodium infection (n=4) (B, up panel). Representative images (B, bottom panel) and the quantitative analysis (C) of microvessel density (MVD) by immunohistochemical staining with antibodies reactive to CD31 were used to characterize the neovascularization in tumor-bearing mice on day 17 after Plasmodium infection. Original magnification: 400×. ***, $p < 0.001$. (D-E) The alginate-encapsulated tumor cell assay was performed according to the description in the “Materials and methods” section (n = 10). Representative images of the alginate beads are shown (D). Quantification of the FITC-dextran uptake by the beads is shown (E). The data are expressed as the mean±SD. ***, $p < 0.001$.

Figure 3

Quantification of TAM infiltration into the tumor tissue. (A-B) Tumor histological specimens were prepared on days 8 and 17 after infection with Plasmodium parasites (n=4) and stained immunohistochemically with a “rat mAb against mouse macrophages” (clone No. RM0029-11H3) (colored by AEC). Representative images are presented (A). The number of infiltrating TAMs was quantified by counting. (B). ***, $p < 0.001$. (C-D) The infiltrating TAMs were sorted by FACS using a FITC-conjugated anti-F4/80 mAb. The proportion of TAMs was analyzed (C). The absolute number of TAMs was quantified per gram of tumor (n=5) (D). All data were analyzed using FlowJo software (7.6.1 version). The purity of the cell populations was between 85% and 90%. (E-F) Hepa1-6 tumor-bearing mice were intraperitoneally injected with Cl2MDP liposomes (300 μl/mouse) at 4, 8 and 13 days after tumor cell inoculation and sacrificed at 16 days. The tumor tissue was dissected, and tumor angiogenesis was examined visually and imaged (E, upper panel). PBS liposomes were used as a control. Neovascularization was examined by immunohistochemical staining with antibodies reactive to CD31, and representative images are shown (E, bottom panel). Infiltrating TAMs were stained with a rat mAb that recognizes mouse macrophages [RM0029-11H3] and imaged (F, medium panel). Original magnification: 400×. Quantitative analyses of the MVD (E right) and TAMs (F, right) were carried out. Data represent the mean MΦ/MVD number per field ± SD (10 fields per tumor sample, 6 tumors per group; 400× magnification, 0.17 mm2/field). ***, $p < 0.001$. (G) Pearson's correlation was used to analyze the correlation between TAM infiltration and the MVD in tumor-bearing mice treated with Cl2MDP liposomes or PBS liposomes. (H-I) Histological tumor specimens were prepared on day 17 after infection with Plasmodium parasites (n=4) and stained immunohistochemically with a “rat mAb against mouse macrophages” and an antibody reactive to CD31. Representative images are shown (H). Original magnification: 400×. The number of infiltrating TAMs and the MVD were quantified by counting. Data represent the number per field ± SD (10 fields per tumor sample, 8 tumors per group; 400× magnification, 0.17 mm2/field). Pearson's correlation was used to analyze the correlation between TAM infiltration and the MVD (I).

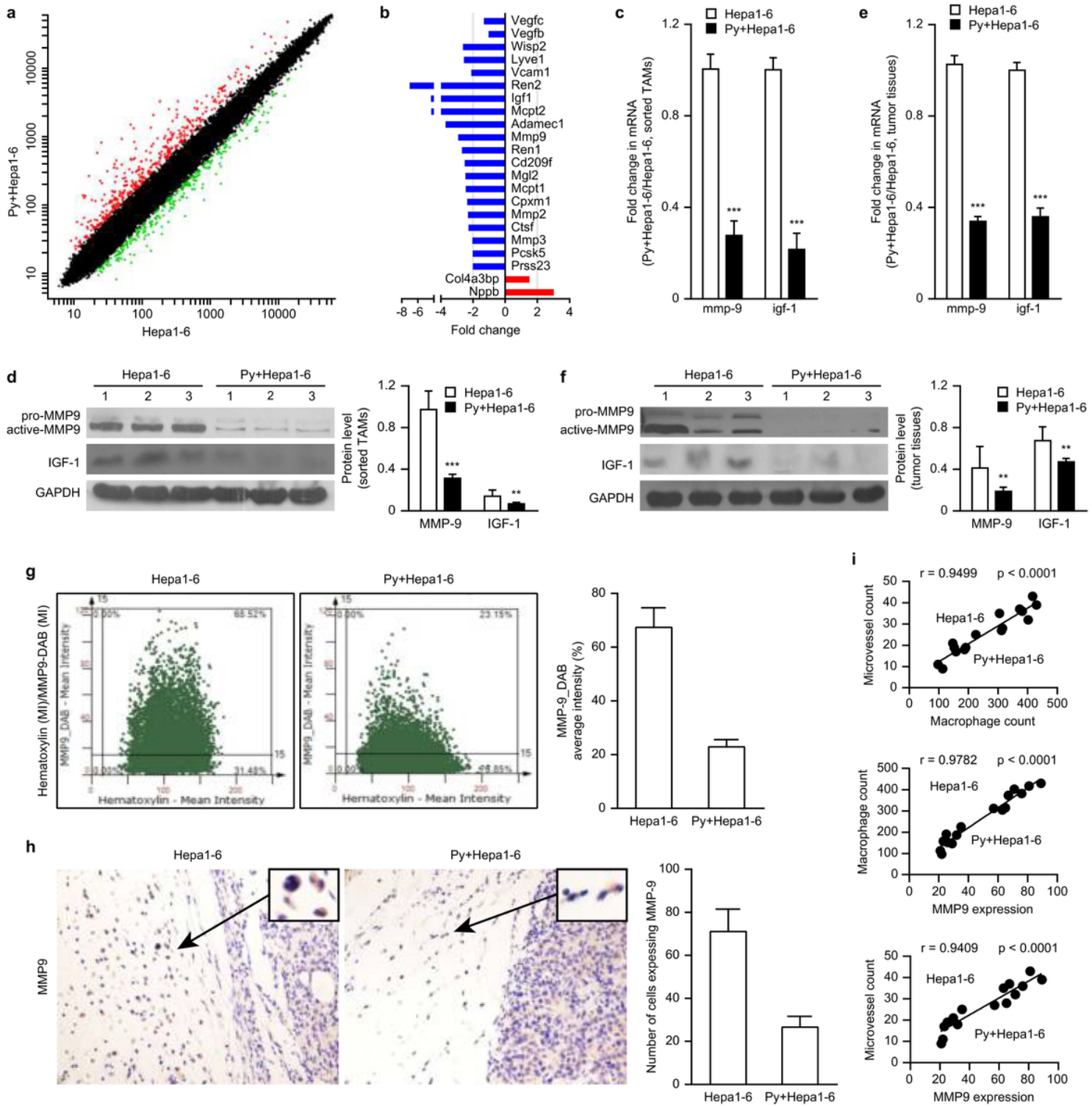

Figure 4

Attenuated MMP-9 expression in the infiltrating TAMs in tumor-bearing mice infected with Plasmodium parasites led to the inhibition of tumor angiogenesis. (A-B) Tumor-bearing mice were sacrificed on day 17 after infection with Plasmodium parasites. TAMs were sorted, RNA was extracted, and then a gene chip (Roche NimbleGen) analysis was carried out to detect the gene expression in TAMs. Genes with a ≥ 2-fold difference in expression and a q-value ≤0.05 were chosen and mapped (A). A molecular annotation system was used to analyze the functions of these differentially expressed genes and the biological

processes involved. Genes associated with tumor angiogenesis with a ≥ 2-fold difference in expression and a q-value ≤ 0.05 were chosen for further analysis (B). (C-F) The relative MMP-9 and IGF-1 mRNA levels in the sorted TAMs (C) and tumor tissue (E) were quantified using qRT-PCR. Western blotting visualized the expression of MMP-9 and IGF-1 in the sorted TAMs (D, left panel) and tumor tissue (F, left panel). Quantitative analysis was performed using ImageJ software to quantify the endogenous MMP-9 and IGF-1 levels in the sorted TAMs (D, right panel) and tumor tissue (F, right panel). (G) A FACS-like tissue cytometer analysis system was applied to analyze the MMP-9 expression by the cells in the tumor margin by immunohistochemical staining with an antibody reactive to MMP-9 on day 17 after infection with Plasmodium parasites. Double-positive scatter plots represent MMP-9-positive cells in scattergrams (left panel). The percentages represent the ratio of MMP-9-positive cells to total cells in the selected area. The mean intensity (MI) represents the average DAB intensity (right panel). (H) Representative images of the MMP-9-positive cells identified by immunohistochemical staining with an antibody reactive to MMP-9 on day 17 after infection with Plasmodium parasites (Original magnification: 400×). The insets show representative cells expressing MMP-9 (left panel) and the number of cells expressing MMP-9 (right panel). (I) A comprehensive analysis of the correlation among MMP-9 expression, MVD, and macrophage infiltration in the tumors from tumor-bearing mice on day 17 after Plasmodium infection compared with that in the tumors from uninfected tumor-bearing mice. $p < 0.05$ was considered significant.

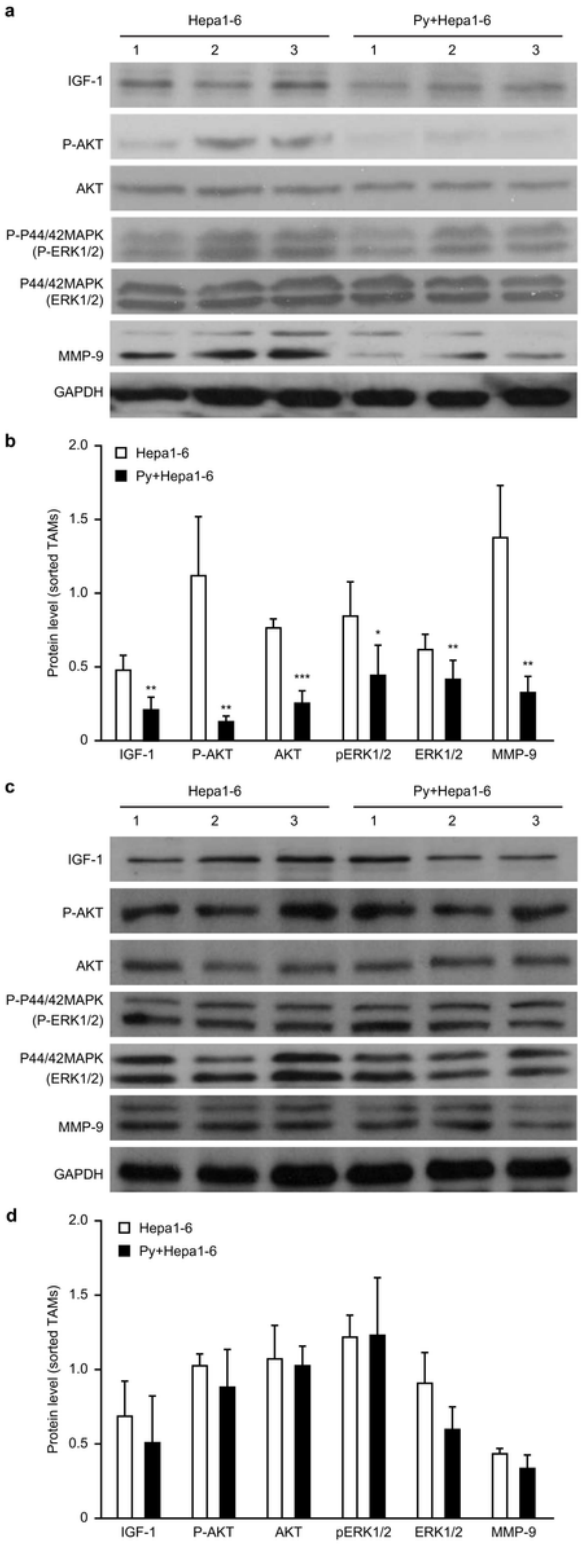

Figure 5

Plasmodium infection attenuated MMP-9 expression by blocking IGF-1R signaling. (A-B) The expression of IGF-1, MMP-9, phosphorylated Akt, total Akt, phosphorylated p42/44 MAPK and total MAPK in the sorted TAMs from tumor-bearing mice on day 17 after Plasmodium infection was detected by immunoblotting (A). Quantitative analysis was performed using ImageJ software to quantify the levels of these signaling proteins in the sorted TAMs (B). (C-D) Plasmodium parasites were killed by chloroquine

on day 8, and AKT signaling and MAPK signaling were examined. Western blotting visualized the restoration of the levels of these signaling proteins (C). Quantitative analysis of signaling proteins in the sorted TAMs from the tumor-bearing mice with Plasmodium infection blocked on day 8 was performed using ImageJ software (D).

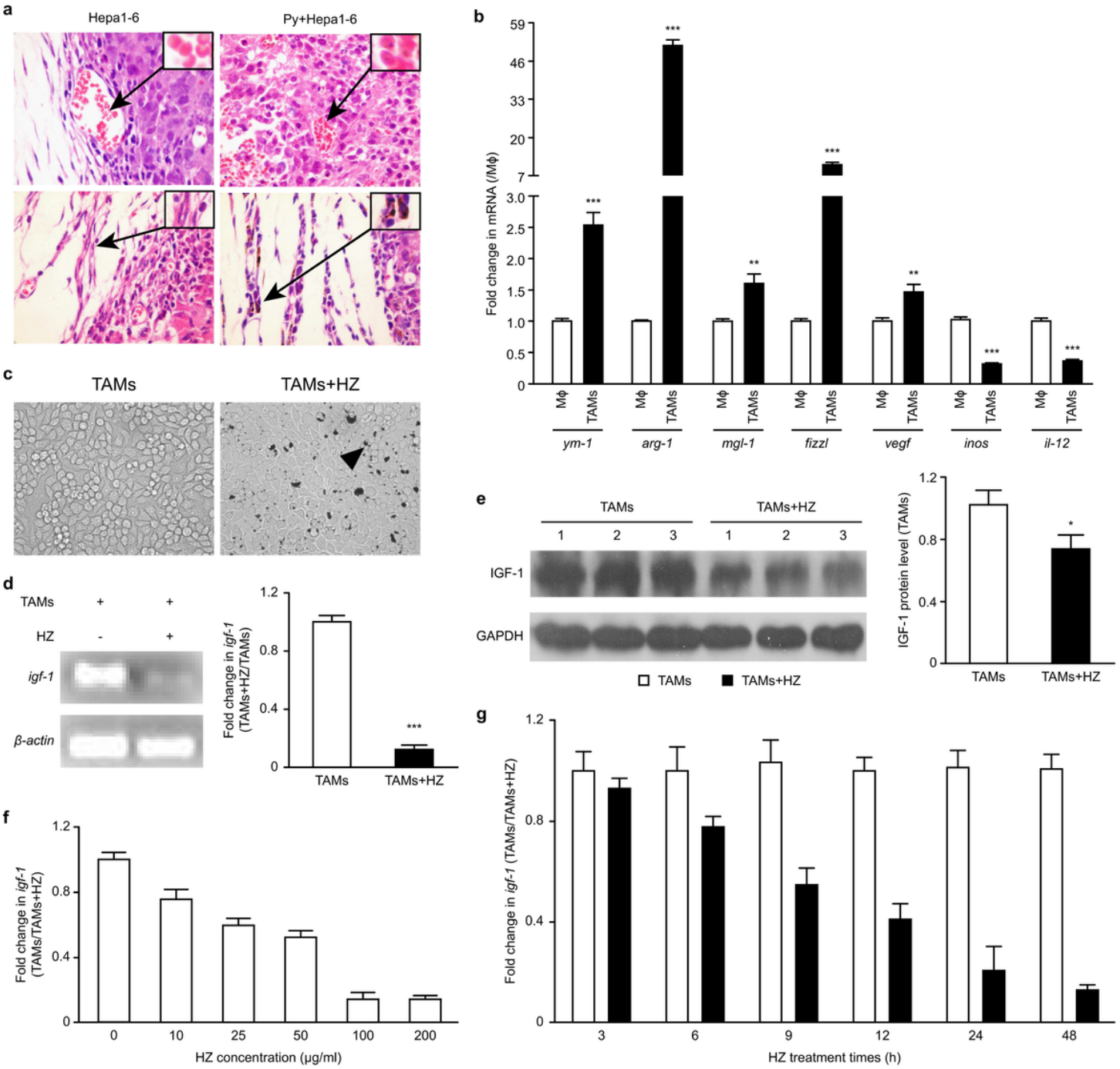

Figure 6

HZ modulated the expression of IGF-1 in TAMs polarized in vitro by coculture. (A) Tumor tissue sections were observed on day 17 after Plasmodium infection (n=4). Parasite-infected red blood cells (iRBCs) could be found in the tumor tissue (upper panel). Representative photos are presented (×1,000 magnification). The insets show representative iRBCs, with the black arrows identifying Plasmodium

parasites in the iRBCs. HZ was found in the TAMs from Hepa1-6 cell-implanted mice infected with Plasmodium parasites (n=4) (bottom panel). Arrows indicate representative cells with HZ accumulation in their cytoplasm. Original magnification: 400×. RAW264.7 cells were plated in the absence or presence of TSN (1:2 dilution). (B-C) Genes associated with TAM phenotype characteristics were analyzed in the induced TAMs using real-time PCR (B). The phagocytosis of HZ by RAW264.7 cells in vitro was also observed (C). Arrows illustrate examples of cells with HZ accumulation in their cytoplasm. Original magnification: 400×. (D-E) Cells were treated with or without HZ (100 μg/ml) in the presence of TSN (1:2 dilution). The level of IGF-1 was analyzed 48 h after co-culture using RT-PCR (D, left panel) and qRT-PCR (D, right panel). The expression of IGF-1 was detected using immunoblotting and quantified by ImageJ software (E). (F-G) In some experiments, the induced TAMs were treated with different doses of HZ. The analysis of IGF-1 mRNA expression was performed using qRT-PCR 48 h later (F). In other experiments, the induced TAMs were exposed to HZ (100 μg/ml) for the indicated time periods. The level of IGF-1 was also analyzed (G). The results are the mean ± SD of the data from the triplicate samples of three independent experiments.

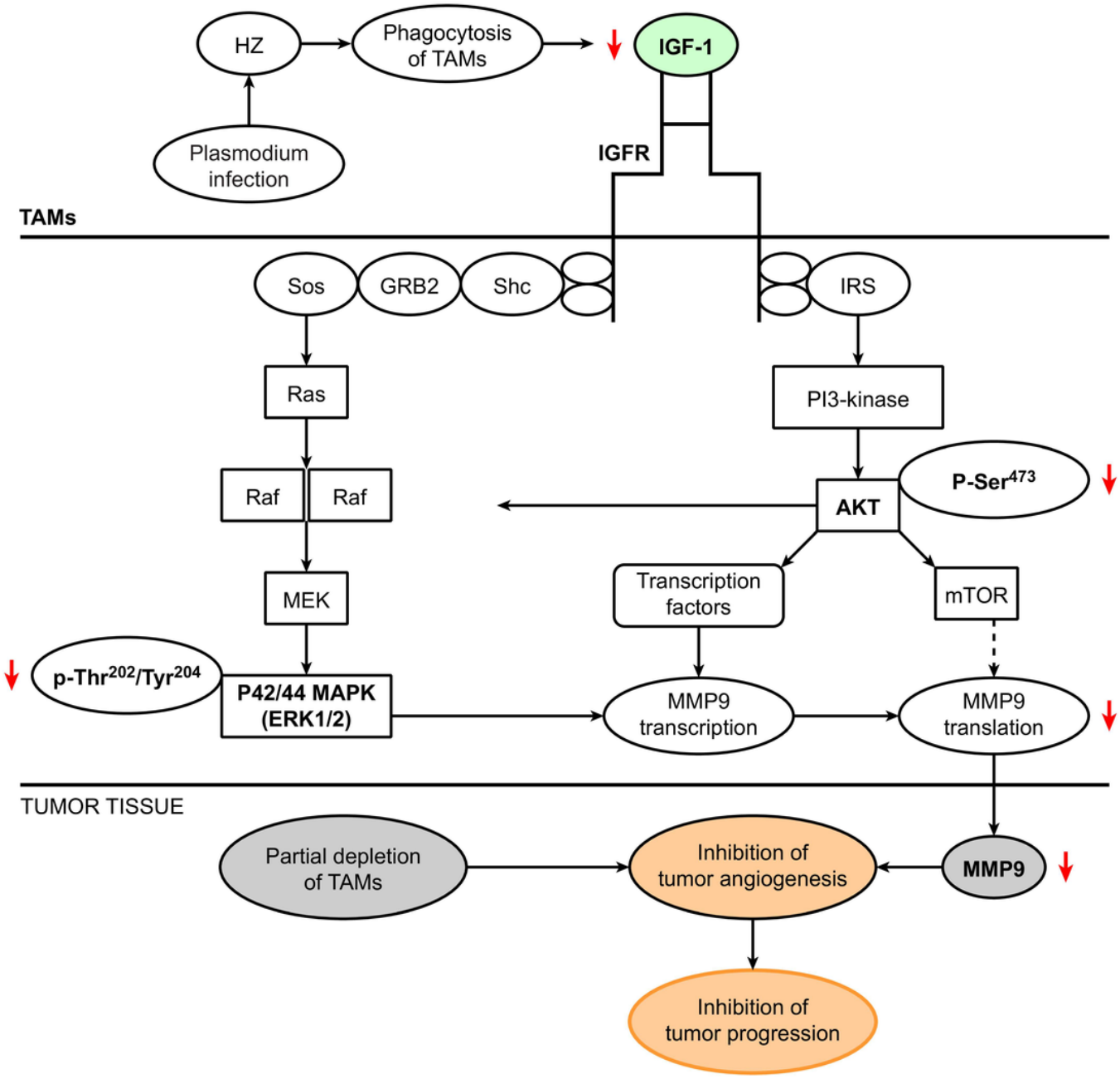

Figure 7

Summary of the mechanisms by which Plasmodium infection inhibits tumor angiogenesis by reducing the infiltration of tumor-associated macrophages (TAMs) and attenuating the expression of MMP-9 in TAMs.

Supplementary Files

This is a list of supplementary files associated with this preprint. Click to download.

- supplementaryMaterial.pdf